Optimal in-Orbit Repositioning of Sun-Pointing Smart Dust

Alessandro A. Quarta*, Giovanni Mengali, Eugenio Denti

Department of Civil and Industrial Engineering, University of Pisa, I-56122, Italy

Abstract

A Smart Dust is a femto-spacecraft with an external surface coated with electrochromic material, which exploits the solar radiation pressure to produce a propulsive acceleration. As the optical properties of the electrochromic material change upon application of a suitable electric voltage, its propulsive acceleration may be modulated, within some limits, without the use of any propellant. This paper analyzes the optimal trajectories of a Sun-pointing Smart Dust, which provides a propulsive acceleration aligned with the Sun-spacecraft direction. In particular, the paper describes the relative motion of a Smart Dust with respect to a conventional spacecraft (the Mother Ship) that covers a heliocentric circular orbit of given radius. The Smart Dust is required to vary periodically its angular position with respect to the Mother Ship using an optimal (minimum time) strategy. This problem is addressed using an indirect approach and the optimal control law is obtained in a closed-form solution. The results discussed in this paper ensure interesting improvements over existing models from the recent literature, including the possibility of obtaining a generic phasing angle of the Smart Dust and to take into account an optimal number of on-off switchings of the electrochromic control system.

Keywords: Sun-pointing Smart Dust, Spacecraft-on-a-chip, Electrochromic control, phasing maneuvers, trajectory optimization

Nomenclature

a	=	SD propulsive acceleration, [$\mathrm{mm/s^2}$]
$\mathcal{A}, \mathcal{B}$	=	auxiliary parameters
$\mathcal{H}$	=	Hamiltonian function
H	=	Heaviside step function
r	=	Sun-SD distance, [au]
t	=	time, [days]
u, v	=	radial and transverse relative velocity, [km/s]
β	=	SD lightness number
λ_i	=	adjoint variable associated with the i-th state
$\mu_\odot$	=	Sun's gravitational parameter, [$\mathrm{au^3/day^2}$]
ϕ	=	phasing angle, [deg]
ρ	=	relative radial distance, [au]
ω	=	angular velocity, [rad/s]

Subscripts

0	=	initial

*Corresponding author

Email addresses: a.quarta@ing.unipi.it (Alessandro A. Quarta), g.mengali@ing.unipi.it (Giovanni Mengali), e.denti@ing.unipi.it (Eugenio Denti)

Published in Acta Astronautica, Vol. 154 January 2019, pp. 278–285. doi: http://dx.doi.org/10.1016/j.actaastro.2018.03.036

c = circular MS orbit
f = final
max = maximum
min = minimum
off = ECS off
on = ECS on

Superscripts

$\star$ = optimal
$\cdot$ = time derivative

1. Introduction

Recent advances in the semiconductor industry have promoted the miniaturization of components used for space applications [1] and inspired the concept of spacecraft-on-a-chip, that is, a Femto Spacecraft (FS) with dimensions comparable to that of a common microchip [2, 3, 4]. A FS presents very interesting characteristics, such as low manufacturing costs as well as cheap launch costs due to a likely employment as a piggy-back payload on more conventional space vehicles. Actually, a number of FSs could also be deployed by the same Mother Ship (MS), as suggested by the recent KickSat project [5] in which more than 100 FSs, with a characteristic dimension of about 3 cm, have been installed inside a 3U CubeSat. In this context, an interesting application is to operate those FSs within a formation (that is, maintaining precise spacing and orientation relative to each other), in order to create an artificial large sensor, such as an antenna, for achieving objectives that would be impossible to reach with a single, conventional, spacecraft.

An interesting and intrinsic feature of a FS consists in its large value of area-to-mass ratio [6, 7]. As a result, the dynamics of a FS is highly affected by the solar radiation pressure, which is usually considered as a perturbation force for a conventional spacecraft. In this sense, the trajectory of a FS can be analyzed with mathematical models that are usually used for describing the dynamics of a solar sail, as thoroughly discussed by Atchison and Peck [8]. However, the main limitation of such a millimeter-scale solar sail without moving parts is in its reduced maneuver capabilities due to a lack of thrust vector control [8]. Indeed, a FS designed to (passively) exploit the photon momentum transfer to obtain thrust, typically provides an outward propulsive acceleration directed along the Sun-FS line. In particular, the propulsive acceleration magnitude of this Sun-pointing FS depends on the Sun-FS distance, the area-to-mass ratio, and the thermo-optical characteristics of the reflective surface [9].

An advanced way to create an active control means consists in covering the FS external surface with electrochromic material [10, 11, 12], which varies its optical properties on application of a suitable electric voltage. Exploiting such a property, Vulpetti et al. [13] have recently investigated the performance of an electrochromic actuator for station-keeping attitude maneuvers of a Sun-pointing solar sail. The same electrochromic material may be used to cover the FS external surface. In that case, these kinds of FSs, which are usually referred to as Smart Dusts (SDs) [14], are able to actively change the propulsive acceleration magnitude by altering the reflectivity coefficient of the electrochromic material. In particular, the reflectivity coefficient of the external surface may take two admissible values only, corresponding to when the Electrochromic Control System (ECS) is either switched off or on. The heliocentric dynamics of a Sun-pointing SD may be analyzed by means of a linear systems approach, and the SD trajectory can be obtained in a closed form using the approach discussed in Ref. [15].

Recently, the linearized dynamics of a Sun-pointing SD, whose distance from the Sun is roughly constant, has been studied using an analytical approach [16]. More precisely, assuming a SD to be deployed by a MS placed on a circular heliocentric orbit, Ref. [16] analyzes the SD-MS relative motion as a function of the generic number of working cycles (that is, the number of on-off switchings of the ECS). The analytical results are then applied to a phasing mission case, where the SD is required to vary its angular position, with respect to that of the MS, along the reference circular orbit. Actually, the closed-form control law discussed in Ref. [16] refers to the simplified case in which the SD may be operated with a single working

cycle only. In fact, according to Ref. [16], the general case in which the ECS completes several working cycles requires an optimal (possibly numerical) approach for evaluating the mission phasing performance.

The aim of this paper is to deal with the phasing mission case using an optimal indirect approach, where the minimum phasing time is obtained as a function of the given phasing angle, without any limitation on the number of working cycles to be used. In particular, this paper shows that the optimal control law can be obtained in a closed form, and the optimal phasing performance is calculated by solving a Two-Point Boundary Value Problem (TPBVP) with three (scalar) unknowns only. In this sense, the model discussed in this paper extends and completes the azimuthal repositioning problem of a Sun-pointing SD along circular orbits introduced in Ref. [16].

The paper is organized as a follows. The next section describes the mission scenario and introduces the mathematical model used to optimize the SD trajectory during the in-orbit repositioning phase, while the SD dynamics is completed by the model discussed in the Appendix. The optimal control law is then used to evaluate, in section 3, the minimum-time phasing trajectories for a set of SDs of given characteristics. Finally, the last section contains some concluding remarks.

2. Problem description

The mission scenario to be analyzed is a special case of that discussed in Ref. [16]. Consider a MS that covers a reference circular orbit of radius r_c around the Sun. At time $t_0 \triangleq 0$ a SD is released by the MS with zero velocity relative to it. The SD is required to perform an orbit phasing [17] by minimizing the flight time. More precisely, the problem is to move the SD along the reference circular orbit of a given angle ϕ_f relative to the MS in the minimum time interval $\Delta t \triangleq t_f - t_0 \equiv t_f$. By definition, a spacecraft performs a phasing ahead maneuver (or behind maneuver) when $\phi_f > 0$ (or $\phi_f < 0$). Accordingly, its position is ahead (or behind) the position it would occupy at time t_f if it were kept on the circular reference orbit, see Fig. 1. In this case the SD can provide an outward radial propulsive acceleration only (that is, an acceleration directed along the Sun-SD line). Therefore, in accordance with the results reported in Ref. [16], the SD is able to carry out a phasing behind maneuver with $\phi_f < 0$, see Fig. 1(b). A phasing ahead maneuver (see Fig. 1(a)) is still possible by means of a drift behind maneuver with a phasing angle $\phi_f \in [-\pi, -2\pi]$ rad. Such a maneuver, however, requires quite large flight times as will be shown later.

2.1. Mathematical preliminaries

When released by the MS, the SD is outward radially propelled with an acceleration magnitude

$$a = \beta \, \frac{\mu_\odot}{r^2} \qquad \text{with} \qquad \beta \in \{\beta_{\min}, \, \beta_{\max}\} \tag{1}$$

where $\mu_\odot$ is the Sun's gravitational parameter, r is the Sun-SD distance, and $\beta > 0$ is a design dimensionless parameter that characterizes the SD performance. In analogy with the classical solar sail literature [9, 18], β is referred to as SD lightness number, that is, the ratio of the propulsive acceleration magnitude to the local Sun's gravitational acceleration.

The lightness number β depends on the area-to-mass ratio and the thermo-optical characteristics of the external reflective surface (the surface that reflects the incoming photons). As long as the degradation effects [19, 20, 21] on the reflecting surface of a Sun-pointing FS are neglected, β is a constant of motion. If instead the external surface is coated with electrochromic material (thus obtaining a SD), the lightness number may take two different values according to whether the ECS is either switched off (in that case $\beta = \beta_{\min} > 0$) or on ($\beta = \beta_{\max} > \beta_{\min}$). Typical values of $\{\beta_{\min}, \, \beta_{\max}\}$ are given by Colombo and McInnes [14] for a low (SD_1), medium (SD_2), and high (SD_3) performance SD, see Tab. 1. In all cases the maximum

	SD_1	SD_2	SD_3
$\beta_{\min}$	0.0134	0.0251	0.0420
$\beta_{\max}$	0.0241	0.0451	0.0756

Table 1: Lightness number of a low (SD_1), medium (SD_2), and high (SD_3) performance SD. Table adapted from Ref. [16] with data taken from Ref. [14].

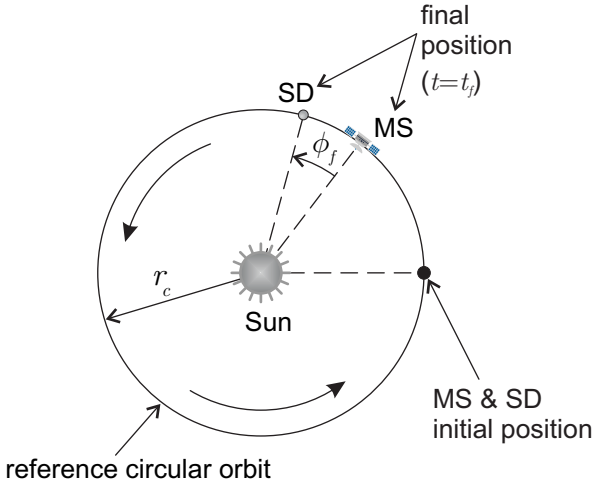

(a) Phasing ahead ($\phi_f > 0$).

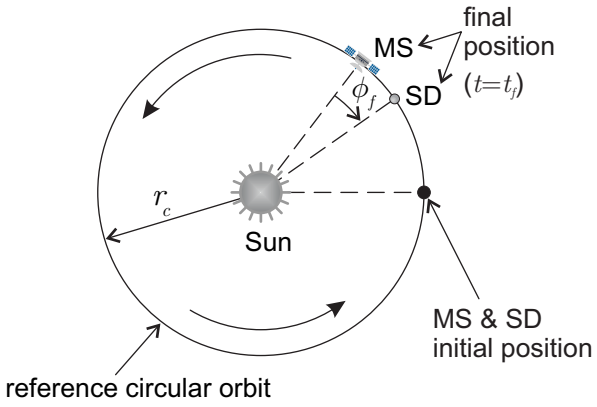

(b) Phasing behind ($\phi_f < 0$).

Figure 1: Conceptual scheme of the mission scenario.

propulsive acceleration magnitude is much below one tenth the local solar gravitational acceleration, so it is reasonable to assume that the SD-Sun distance remains close to r_c (the initial value) for all the phasing trajectory. The heliocentric SD dynamics may therefore be described with the linearized model discussed in Ref. [16], which follows the set of equations introduced by McInnes [22] for a solar sail-based mission scenario. In particular, the soundness of the approximate model discussed in Ref. [22] has been checked in Ref. [23] using a set of non-linear equations of motions.

With reference to the conceptual scheme shown in Fig. 2, the SD linearized equations of motion along the heliocentric circular orbit of radius r_c are

$$\dot{\rho} = u \tag{2}$$

$$\dot{\phi} = \frac{v}{r_c} \tag{3}$$

$$\dot{u} = 2\,\omega\,v + 3\,\omega^2\,\rho + \beta\,\frac{\mu_\odot}{r_c^2} \tag{4}$$

$$\dot{v} = -2\,\omega\,u \tag{5}$$

where $\omega = \sqrt{\mu_\odot / r_c^3}$ is the MS (constant) angular velocity, $\rho \triangleq r - r_c$ is the SD-MS relative radial distance (with $|\rho| / r_c \ll 1$), ϕ is the SD-MS relative angular coordinate, and u (or v) is the radial (or transverse) component of the SD-MS relative velocity.

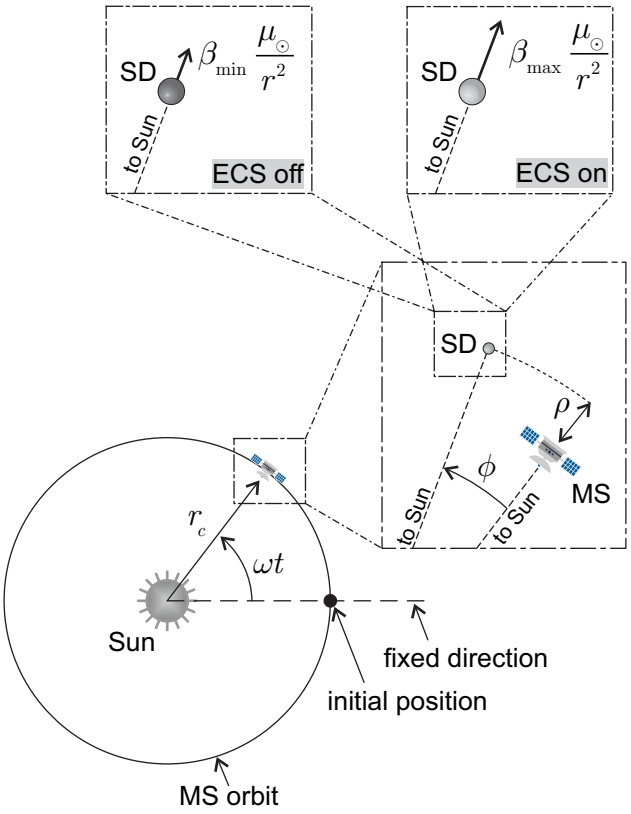

Figure 2: Reference frame. Figure adapted from Ref. [16].

The previous equations of motion may be solved in closed analytical form once the control law $\beta = \beta(t)$ is given (recall that $\beta = \{\beta_{\min}, \beta_{\max}\}$). This allows the SD-MS relative trajectory to be found, as is thoroughly discussed in Ref. [16]. The main results are summarized in the Appendix and represent the starting point for the optimal control problem discussed in the next section.

2.2. Trajectory optimization

While the MS tracks a circular Keplerian orbit, the phasing problem is to vary the SD angular position (relative to the MS) of a given angle ϕ_f in the minimum time interval $\Delta t = t_f$. This amounts to finding the optimal time-variation of the SD lightness number $\beta = \beta(t)$ that minimizes the time t_f necessary to transfer the SD from its initial state, given by Eq. (A.2), to a final state defined as

$$\rho(t_f) = 0 \quad , \quad \phi(t_f) = \phi_f \quad , \quad u(t_f) = v(t_f) = 0 \tag{6}$$

see Fig. 1. Note that, from Eq. (A.5), the condition $v(t_f) = 0$ is naturally met when $\rho(t_f) = 0$. Accordingly, the scalar constraints, to be enforced at the final time t_f, are reduced to three, or

$$\rho(t_f) = 0 \quad , \quad \phi(t_f) = \phi_f \quad , \quad u(t_f) = 0 \tag{7}$$

The problem is therefore to maximize the performance index

$$J \triangleq -t_f \tag{8}$$

which can be tackled with an indirect approach [24, 25]. To that end, the Hamiltonian function $\mathcal{H}$ is defined as

$$\mathcal{H} \triangleq \lambda_\rho\, u + \frac{\lambda_\phi\, v}{r_c} + \lambda_u \left(2\,\omega\, v + 3\,\omega^2\, \rho + \beta\, \frac{\mu_\odot}{r_c^2} \right) - 2\,\lambda_v\, \omega\, u \tag{9}$$

where $\{\lambda_\rho,\, \lambda_\phi,\, \lambda_u,\, \lambda_v\}$ are the adjoint variables associated with the SD state $\{\rho,\, \phi,\, u,\, v\}$. The time derivatives of the adjoint variables are given by the Euler-Lagrange equations

$$\dot{\lambda}_\rho = -\frac{\partial \mathcal{H}}{\partial \rho} = -3\,\omega^2\, \lambda_u \tag{10}$$

$$\dot{\lambda}_\phi = -\frac{\partial \mathcal{H}}{\partial \phi} = 0 \tag{11}$$

$$\dot{\lambda}_u = -\frac{\partial \mathcal{H}}{\partial u} = 2\,\omega\, \lambda_v - \lambda_\rho \tag{12}$$

$$\dot{\lambda}_v = -\frac{\partial \mathcal{H}}{\partial v} = -2\,\omega\, \lambda_u - \frac{\lambda_\phi}{r_c} \tag{13}$$

with initial conditions

$$\lambda_\rho(t_0) = \lambda_{\rho_0} \quad , \quad \lambda_\phi(t_0) = \lambda_{\phi_0} \quad , \quad \lambda_u(t_0) = \lambda_{u_0} \quad , \quad \lambda_v(t_0) = \lambda_{v_0} \tag{14}$$

where $\{\lambda_{\rho_0},\, \lambda_{\phi_0},\, \lambda_{u_0},\, \lambda_{v_0}\}$ are four unknown parameters whose values are the output of the TPBVP. Note that, according to Eq. (9), the Hamiltonian does not explicitly depend on time and, therefore, $\mathcal{H}$ is a constant of motion [24], that is, $\mathcal{H}(t_0) = \mathcal{H}(t_f)$. Therefore, enforcing the transversality condition

$$\mathcal{H}(t_f) = 1 \tag{15}$$

and taking into account Eqs. (9) and (A.2), viz.

$$\mathcal{H}(t_0) = \lambda_{u_0}\, \beta_0\, \frac{\mu_\odot}{r_c^2} \tag{16}$$

the value of λ_{u_0} is obtained as

$$\lambda_{u_0} = \frac{r_c^2}{\mu_\odot\, \beta_0} \tag{17}$$

where $\beta_0 = \beta(t_0)$ is the initial value of the SD lightness number, that is, the initial value of the control variable.

The Euler-Lagrange equations (10)–(13) with the initial conditions given by Eqs (14) can be solved with standard methods, and the result is

$$\lambda_\rho = \lambda_{\rho_0}\, \left[4 - 3\cos(\omega\, t)\right] + \frac{6\,\lambda_{\phi_0}}{r_c}\, \left[\omega\, t - \sin(\omega t)\right] - 3\,\omega\,\lambda_{u_0}\, \sin(\omega t) - 12\,\omega\,\lambda_{v_0}\, \sin^2\left(\frac{\omega t}{2}\right) \tag{18}$$

$$\lambda_\phi = \lambda_{\phi_0} \tag{19}$$

$$\lambda_u = -\frac{\lambda_{\rho_0}}{\omega}\, \sin(\omega t) + \frac{2\,\lambda_{\phi_0}\, \left[\cos(\omega t) - 1\right]}{\omega\, r_c} + \lambda_{u_0}\, \cos(\omega t) + 2\,\lambda_{v_0}\, \sin(\omega t) \tag{20}$$

$$\lambda_v = \frac{4\,\lambda_{\rho_0}}{\omega}\, \sin^2\left(\frac{\omega t}{2}\right) + \frac{\lambda_{\phi_0}}{\omega\, r_c}\, \left[3\omega t - 4\sin(\omega t)\right] - 2\lambda_{u_0} \sin(\omega t) + \lambda_{v_0} \left[1 - 8\sin^2\left(\frac{\omega t}{2}\right)\right] \tag{21}$$

Note that λ_ϕ is a constant of motion and its value coincides with λ_{ϕ_0}, see Eqs. (11) and (19). In particular, the right-hand side of Eq. (20) plays an important role in the definition of the optimal control law. In fact,

from the Pontryagin's maximum principle, the optimal control law $\beta = \beta(t)$, to be selected in the domain of feasible values of lightness number $\beta \in \{\beta_{\min}, \beta_{\max}\}$, is such that, at any time, the Hamiltonian $\mathcal{H}$ is an absolute maximum. Since $\mathcal{H}$ is a linear function of β, see Eq. (9), the optimal control law is

$$\beta(t) = \beta^\star(t) \triangleq \begin{cases} \beta_{\min} & \text{if} \quad \lambda_u(t) < 0 \\ \beta_{\max} & \text{if} \quad \lambda_u(t) \geq 0 \end{cases} \tag{22}$$

Recalling that $\beta_0 > 0$, from Eqs. (17) and (22) the initial value of the SD lightness number is

$$\beta_0 = \beta_{\max} \tag{23}$$

and, therefore, the initial value of the adjoint variable λ_u is

$$\lambda_{u_0} = \frac{r_c^2}{\mu_\odot \, \beta_{\max}} \tag{24}$$

Equation (23) states that the ECS is to be switched on at the beginning of the phasing maneuver. Taking into account Eq. (24), the expression of $\lambda_u(t)$ given by Eq. (20) can be rewritten in a more compact form as

$$\lambda_u(t) = \frac{r_c^2}{\mu_\odot \, \beta_{\max}} \cos(\omega t) + \mathcal{A} \, [\cos(\omega t) - 1] + \mathcal{B} \sin(\omega t) \tag{25}$$

where $\mathcal{A}$ and $\mathcal{B}$ are two constant parameters depending on λ_{ρ_0}, λ_{ϕ_0} and λ_{v_0}, viz.

$$\mathcal{A} \triangleq \frac{2 \, \lambda_{\phi_0}}{\omega \, r_c} \qquad , \qquad \mathcal{B} \triangleq 2 \, \lambda_{v_0} - \frac{\lambda_{\rho_0}}{\omega} \tag{26}$$

Note that, when $\mathcal{A}$ and $\mathcal{B}$ are fixed, the optimal control law is fully obtained by substituting Eq. (25) into Eq. (22). In other terms, the TPBVP associated with the minimum time problem consists in finding the triplet $\{\mathcal{A}, \mathcal{B}, t_f\}$ such that the boundary conditions of Eqs. (7) are all met.

In general, the TPBVP can be solved by means of a hybrid numerical technique that combines the use of genetic algorithms to obtain a rough estimate of the adjoint variables, with gradient-based and direct methods to refine the solution [26]. In this case, however, the analytical solution of the SD heliocentric dynamics at the final time can be calculated by Eqs. (A.4) for an assigned control law $\beta = \beta(t)$. The associated TPBVP can therefore be translated into the solution of a system of three non-linear scalar equations. This is possible using the following approach: 1) Make a first guess of the unknowns parameters $\{\mathcal{A}, \mathcal{B}, t_f\}$; 2) Calculate the set of time instants t_i, with $i > 1$, in which $\lambda_u(t_i) = 0$, by evaluating the roots of the right-hand side of Eq. (25) in the interval $t \in [0, \, t_f]$; 3) Find the time instants t_{on_i} (or t_{off_i}) in which the ESC is switched-on (or switched-off) using the equation

$$t_i = \begin{cases} t_{\text{on}_i} & \text{if} \quad \dot{\lambda}_u(t_i) > 0 \\ t_{\text{off}_i} & \text{if} \quad \dot{\lambda}_u(t_i) < 0 \end{cases} \tag{27}$$

where the time derivative $\dot{\lambda}_u(t)$ is obtained from Eq. (25) as

$$\dot{\lambda}_u(t) = -\frac{\omega \, r_c^2}{\mu_\odot \, \beta_{\max}} \sin(\omega t) - \mathcal{A} \, \omega \sin(\omega t) + \mathcal{B} \, \omega \cos(\omega t) \tag{28}$$

4) Find the final value of $\rho(t_f)$, $\phi(t_f)$, and $u(t_f)$ using Eqs. (A.4); 5) Check whether the final constraints of Eqs. (7) are met and, if necessary, return to step 2 with a different set of $\{\mathcal{A}, \mathcal{B}, t_f\}$.

The optimal control law given by Eq. (22) has been simulated in a number of phasing missions, as is discussed in the next section.

3. Mission application

The previous trajectory optimization has been applied to study the in-orbit repositioning problem of a low performance (SD_1), medium performance (SD_2), and high performance (SD_3) smart dust, whose characteristics are summarized in Tab. 1. The MS is chosen to cover a reference heliocentric circular orbit of radius $r_c = 1\,\text{au}$.

In order to validate the mathematical model, the phasing problem has been parametrically studied by considering a number of different values of final phasing angle ϕ_f. According to Ref. [16], when the ECS is always switched-on, the phasing angle ϕ_f reaches a minimum value (or a maximum value $|\phi_f|$) given by

$$\phi_{f_{\min}} = -4\,k\,\pi\,\beta_{\max} \tag{29}$$

where $k \in \mathbb{N}^+$. The corresponding flight time is

$$t_f = k\,T_c \tag{30}$$

where $T_c = 2\pi/\omega$ is the MS orbital period. On the other hand, when the ECS is always switched-off, the phasing angle reaches a maximum value (or a minimum value of $|\phi_f|$) given by

$$\phi_{f_{\max}} = -4\,k\,\pi\,\beta_{\min} \tag{31}$$

where the flight time is given, again, by Eq. (30). For example, when $k = 1$ (the minimum admissible value of k), the value of $\phi_{f_{\min}}$ and $\phi_{f_{\max}}$ is shown in Tab. 2.

	SD_1	SD_2	SD_3
$\phi_{f_{\min}}$ [deg]	-17.352	-18.072	-30.24
$\phi_{f_{\max}}$ [deg]	-9.648	-32.472	-54.432

Table 2: Minimum ($\phi_{f_{\min}}$) and maximum ($\phi_{f_{\max}}$) value of the phasing angle when $k = 1$ and $t_f = T_c$.

Assuming $\phi_f \in (\phi_{f_{\min}}, \phi_{f_{\max}})$, where the pairs $\{\phi_{f_{\min}}, \phi_{f_{\max}}\}$ are given in Tab. 2 as a function of the SD performance, it is possible to evaluate the minimum flight time using the procedure described in the previous section. The results are shown in Fig. 3 for the three SDs reported in Tab. 1. In particular, the black circles placed in the figure at $t_f/T_c = 1$ illustrate the cases in which the ECS is switched-on (or switched-off) during the whole phasing maneuver. In all other cases, that is, when $\phi_f \in (\phi_{f_{\min}}, \phi_{f_{\max}})$, the phasing maneuvers is constituted by arcs with either $\beta = \beta_{\max}$ or $\beta = \beta_{\min}$ in accordance with the optimal control law given by Eq. (22). Figures 3(a)–3(c) show that each SD is able to perform an orbit phasing maneuver (with a minimum and a maximum value of ϕ_f given by Tab. 2) with an optimal flight time less than one orbital period T_c of the MS. This represents a clear improvement of the (non optimal) result discussed in Ref. [16], where a phasing maneuver with the same value of ϕ_f was obtained with a flight time $t_f > T_c$. The total time interval Δt_{on} in which the ECS is switched-on (that is, the sum of the time intervals in which $\beta = \beta_{\max}$) varies with the desired phasing angle ϕ_f, as is clearly illustrated in Fig. 4. Finally, Fig. 5 shows the maximum value $|\rho|_{\max}$ of the relative radial distance between SD and MS. Recall that the linearized equations of motions have been obtained under the assumption that $|\rho|/r_c \ll 1$, which is indeed confirmed by the simulations.

The effectiveness of the discussed method may be better appreciated with a more complex mission, which requires a total time greater than T_c. For exemplary purposes, consider the SD_1 case, whose mission is to be directed toward the L_5 Lagrangian point. This may be seen as a special case of a phasing maneuver in which the phasing angle to reach is equal to $-60\,\text{deg}$. The simulation results are reported in Fig. 6. It should be noted that the SD repeatedly approaches the MS trajectory without reaching it until the mission end, when all of the boundary conditions of Eqs. (6) are simultaneously met. The total mission time is 1357 days, while the complexity of the control law, with a number of working cycles, is illustrated in Fig. 7. Finally, it is worth noting that a phasing ahead condition may be obtained with a sufficiently long mission. For example, the langrangian point L_4, characterized by a phasing angle of 60 deg, may be reached through a phasing behind trajectory with $\phi_f = -300\,\text{deg}$. This is clearly illustrated in Fig. 8, which shows the trajectory tracked by a SD_3. In this case the total mission time is 2098 days, while the corresponding control law is reported in Fig. 9.

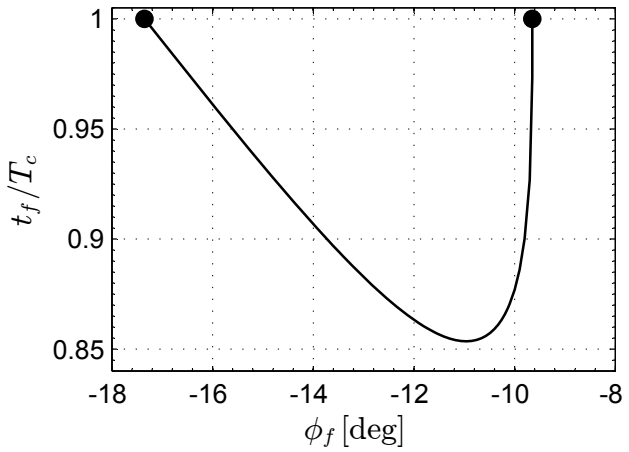

(a) Low performance (SD_1).

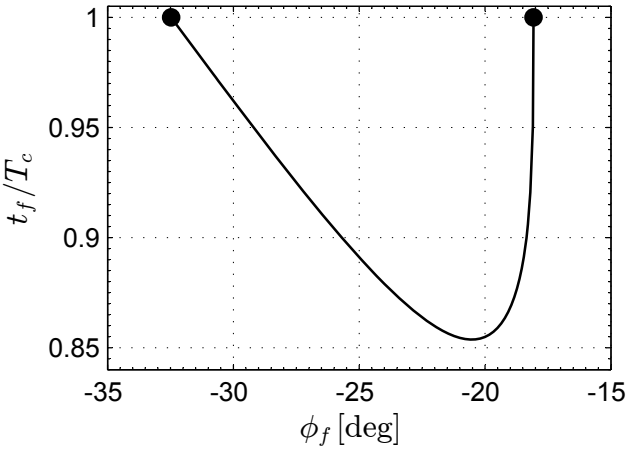

(b) Medium performance (SD_2).

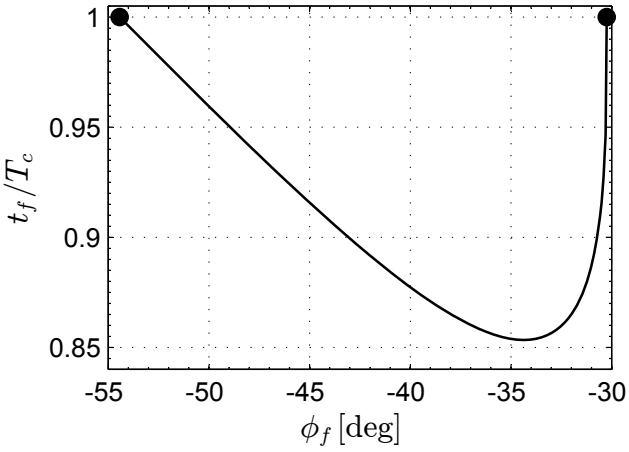

(c) High performance (SD_3).

Figure 3: Minimum phasing time t_f as a function of the phasing angle ϕ_f (see Tab. 2) and the SD performance (see Tab. 1).

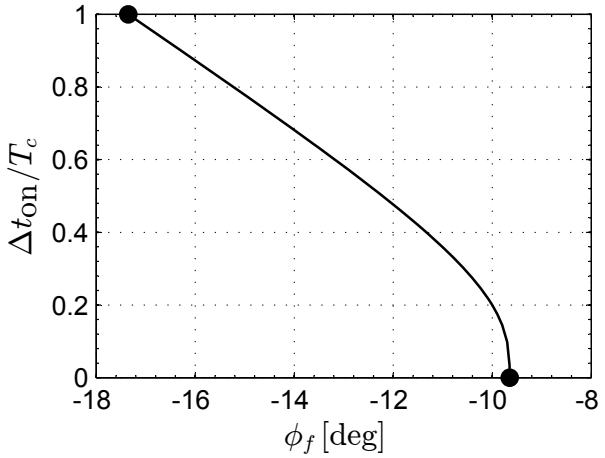

(a) Low performance (SD_1).

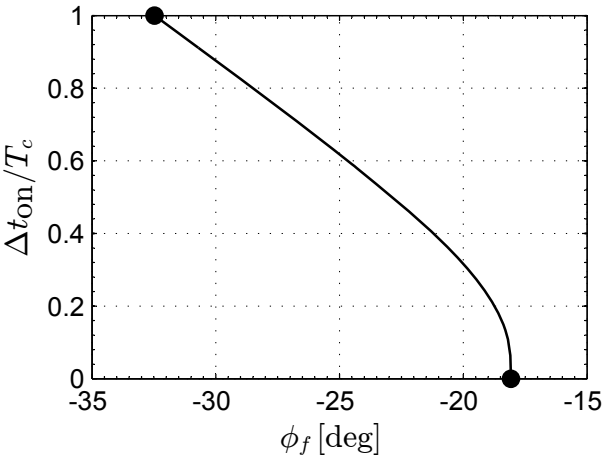

(b) Medium performance (SD_2).

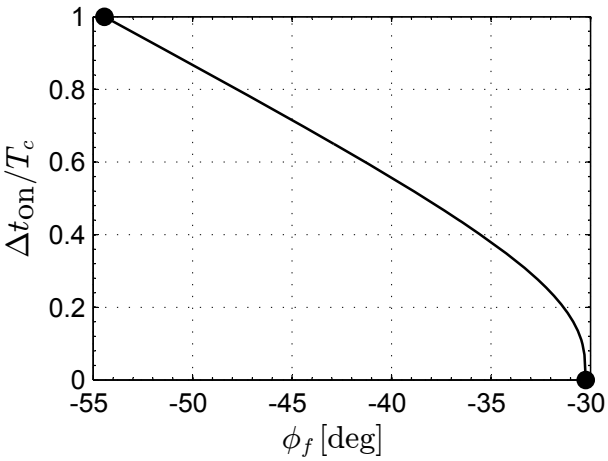

(c) High performance (SD_3).

Figure 4: Time interval Δt_{on} in which the ECS is switched-on as a function of the phasing angle ϕ_f.

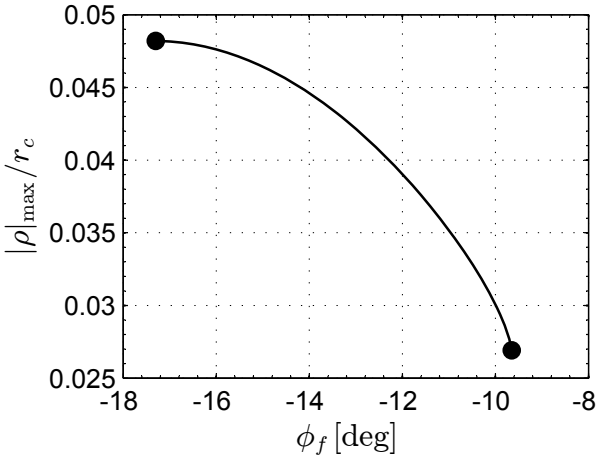

(a) Low performance (SD_1).

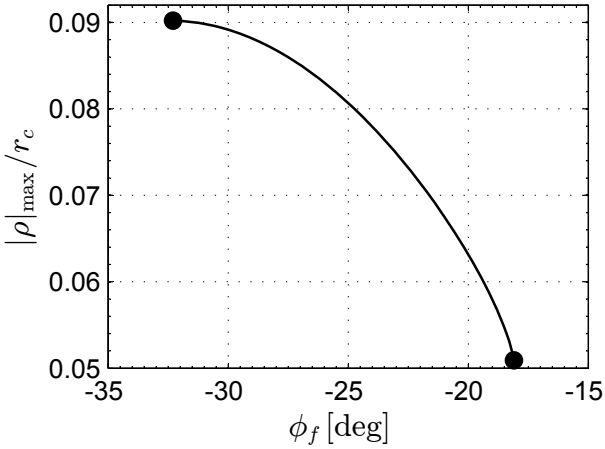

(b) Medium performance (SD_2).

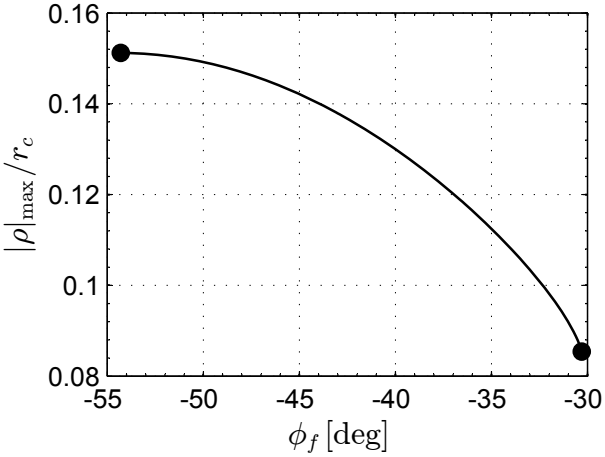

(c) High performance (SD_3).

Figure 5: Maximum relative radial distance between SD and MS as a function of the phasing angle ϕ_f.

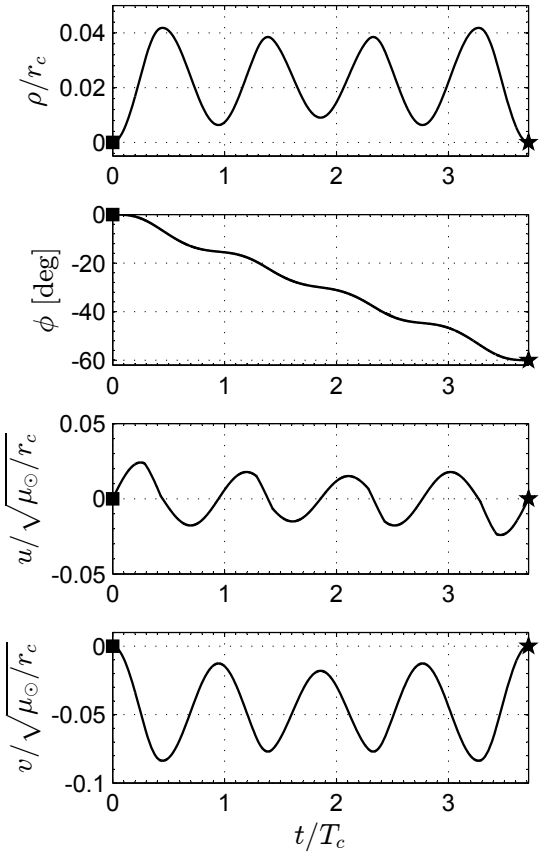

(a) State variables.

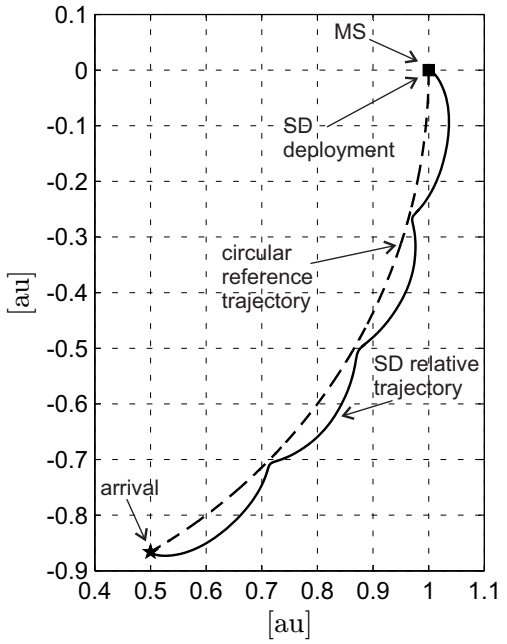

(b) Relative trajectory.

Figure 6: Optimal phasing mission with $\phi_f = -60\,\text{deg}$ for the SD_1 case. The black square coincides with the SD deployment, and the black star with the mission end.

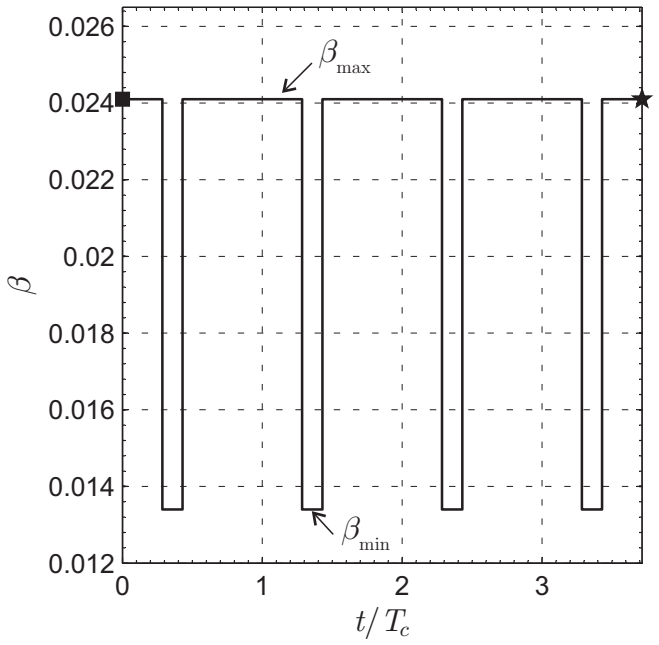

Figure 7: Optimal control law for a phasing mission with $\phi_f = -60\,\text{deg}$ using a SD_1 spacecraft. The black square coincides with the SD deployment, and the black star with the mission end.

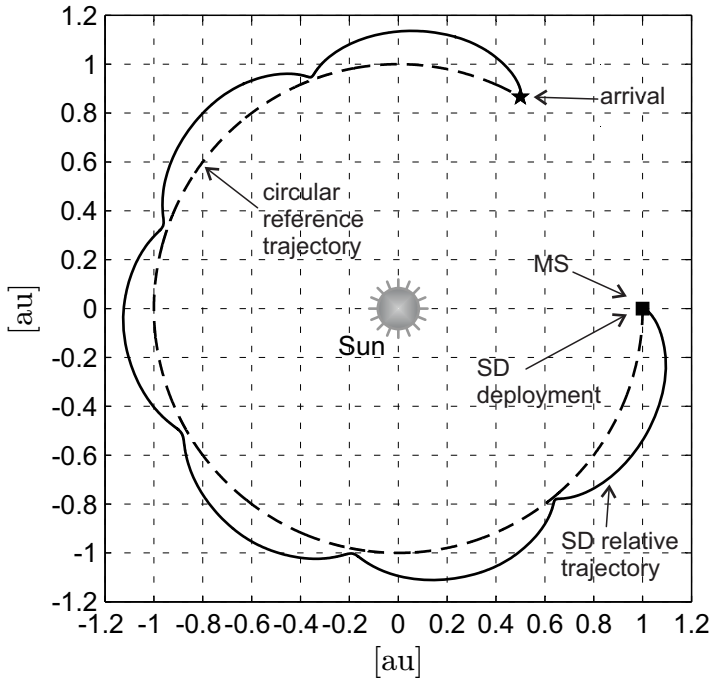

Figure 8: Phasing mission with $\phi_f = 60\,\text{deg}$ using a SD_3 spacecraft (relative trajectory).

4. Conclusions

This paper has studied, from an optimal viewpoint, the phasing maneuver of a Smart Dust that covers a heliocentric circular orbit of given radius. The optimal control law is obtained in a fully analytical form

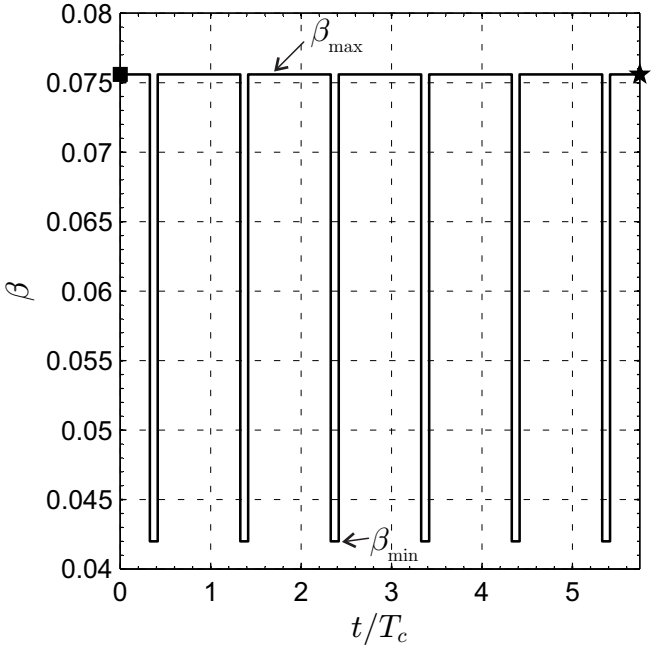

Figure 9: Optimal control law for a phasing mission with $\phi_f = 60\,\text{deg}$ using a SD_3 spacecraft.

by means of an indirect approach. Starting from the recent results about the solution of the Smart Dust linearized dynamics with a general control law, the new approach allows the solution of the associated two-point boundary value problem to be found in an easy and efficient way. In particular, the paper illustrates a practical method for calculating the adjoint variables, which is usually a difficult task in indirect problems. The Smart Dust phasing maneuver is solved for a generic value of the phasing angle and as a function of the Smart Dust performance. In addition, the control law defines the optimal number of on-off switchings of the electrochromic control system. The obtained results complete the motion analysis of a Sun-pointing Smart Dust in a heliocentric mission scenario. A future extension of the results should take into account the presence of a possible circumferential component of the Smart Dust propulsive acceleration. However, a situation in which the thrust is not aligned with the radial direction is difficult to obtain with a Smart Dust as it requires a complex design of its mass distribution and external surface coating.

Appendix A. Smart dust trajectory equation

The linearized dynamics of a SD, see Eqs. (2)–(5), may be solved using the linear systems approach discussed in Ref. [16]. A brief summary is below reported for the sake of completeness. Assuming the ECS to be switched on (or off) at time t_{on_i} (or t_{off_i}), with $i \in \mathbb{N}$ and $t_{\text{off}_i} > t_{\text{on}_i}$, the time variation of the SD lightness number β can be written as

$$\beta(t) = \beta_{\min} + (\beta_{\max} - \beta_{\min}) \left[\sum_{i=1}^{n} H(t - t_{\text{on}_i}) - \sum_{i=1}^{n} H(t - t_{\text{off}_i}) \right] \tag{A.1}$$

where $n \geq 1$ is the number of working cycles of the electrochromic material (that is, the number of on-off switchings of the ECS), whereas $H(y)$ is the Heaviside step function, that is, $H(y) = 0$ if $y < 0$, and $H(y) = 1$ if $y \geq 0$.

Since the SD at $t_0 = 0$ leaves the MS with zero relative velocity, the initial conditions are

$$\rho(t_0) = 0 \quad , \quad \phi(t_0) = 0 \quad , \quad u(t_0) = v(t_0) = 0 \tag{A.2}$$

The differential equations (2)–(5) with the control law (A.1) can be solved with standard methods, and the result is

$$\begin{bmatrix}\rho(t)\\ \phi(t)\\ u(t)\\ v(t)\end{bmatrix} = (\beta_{\max}-\beta_{\min})\sum_{i=1}^{n} H(t-t_{\mathrm{on}_i}) \begin{bmatrix} r_c\,[1-\cos(\omega t-\omega t_{\mathrm{on}_i})] \\ 2\,[\sin(\omega t-\omega t_{\mathrm{on}_i})-\omega t+\omega t_{\mathrm{on}_i}] \\ \omega\, r_c\,\sin(\omega t-\omega t_{\mathrm{on}_i}) \\ 2\,\omega\, r_c\,[\cos(\omega t-\omega t_{\mathrm{on}_i})-1] \end{bmatrix} +$$

$$-(\beta_{\max}-\beta_{\min})\sum_{i=1}^{n} H(t-t_{\mathrm{off}_i}) \begin{bmatrix} r_c\,[1-\cos(\omega t-\omega t_{\mathrm{off}_i})] \\ 2\,[\sin(\omega t-\omega t_{\mathrm{off}_i})-\omega t+\omega t_{\mathrm{off}_i}] \\ \omega\, r_c\,\sin(\omega t-\omega t_{\mathrm{off}_i}) \\ 2\,\omega\, r_c\,[\cos(\omega t-\omega t_{\mathrm{off}_i})-1] \end{bmatrix} + \beta_{\min} \begin{bmatrix} r_c\,[1-\cos(\omega t)] \\ 2\,[\sin(\omega t)-\omega t] \\ \omega\, r_c\,\sin(\omega t) \\ 2\,\omega\, r_c\,[\cos(\omega t)-1] \end{bmatrix} \tag{A.3}$$

Upon completion of the last working cycle, when the ECS is eventually switched off, the SD dynamics is given by the following relationships

$$\begin{bmatrix}\rho(t)\\ \phi(t)\\ u(t)\\ v(t)\end{bmatrix} = \beta_{\min} \begin{bmatrix} r_c\,[1-\cos(\omega t)] \\ 2\,[\sin(\omega t)-\omega t] \\ \omega\, r_c\,\sin(\omega t) \\ 2\,\omega\, r_c\,[\cos(\omega t)-1] \end{bmatrix} + (\beta_{\max}-\beta_{\min})\sum_{i=1}^{n} \begin{bmatrix} -r_c\,\cos(\omega t-\omega t_{\mathrm{on}_i}) \\ 2\,[\sin(\omega t-\omega t_{\mathrm{on}_i})+\omega t_{\mathrm{on}_i}] \\ \omega\, r_c\,\sin(\omega t-\omega t_{\mathrm{on}_i}) \\ 2\,\omega\, r_c\,\cos(\omega t-\omega t_{\mathrm{on}_i}) \end{bmatrix} +$$

$$-(\beta_{\max}-\beta_{\min})\sum_{i=1}^{n} \begin{bmatrix} -r_c\,\cos(\omega t-\omega t_{\mathrm{off}_i}) \\ 2\,[\sin(\omega t-\omega t_{\mathrm{off}_i})+\omega t_{\mathrm{off}_i}] \\ \omega\, r_c\,\sin(\omega t-\omega t_{\mathrm{off}_i}) \\ 2\,\omega\, r_c\,\cos(\omega t-\omega t_{\mathrm{off}_i}) \end{bmatrix} \tag{A.4}$$

According to Eqs. (A.3) and (A.4), the time variation of v becomes

$$v(t) = -2\,\omega\,\rho(t) \tag{A.5}$$

and is therefore simply proportional to the (relative) radial distance $\rho(t)$.

References

[1] L. Bilhaut, L. Duraffourg, Assessment of nanosystems for space applications, Acta Astronautica 65 (9-10) (2009) 1272–1283, doi: 10.1016/j.actaastro.2009.03.066.

[2] D. J. Barnhart, T. Vladimirova, A. M. Baker, M. N. Sweeting, A low-cost femtosatellite to enable distributed space missions, Acta Astronautica 64 (11–12) (2009) 1123–1143, doi: 10.1016/j.actaastro.2009.01.025.

[3] D. J. Barnhart, T. Vladimirova, M. N. Sweeting, Satellite-on-a-chip feasibility for future distributed space missions, in: Proceedings of MNT for Aerospace Applications, CANEUS2006, Toulouse, France, 2006, paper CANEUS 2006-11045.

[4] D. J. Barnhart, T. Vladimirova, M. N. Sweeting, Very-small-satellite design for distributed space missions, Journal of Spacecraft and Rockets 44 (6) (2007) 1294–1306, doi: 10.2514/1.28678.

[5] Z. Manchester, M. Peck, A. Filo, KickSat: A crowd-funded mission to demonstrate the world's smallest spacecraft, in: Proceedings of the AIAA/USU Conference on Small Satellites, Logan, Utah, 2013, paper SSC13-IX-5.

[6] C. Colombo, C. Lücking, C. R. McInnes, Orbital dynamics of high area-to-mass ratio spacecraft with J_2 and solar radiation pressure for novel Earth observation and communication services, Acta Astronautica 81 (2012) 137—50, doi: 10.1016/j.actaastro.2012.07.009.

[7] C. Colombo, C. R. McInnes, Orbit design for future spacechip swarm missions in a planetary atmosphere, Acta Astronautica 75 (2012) 25–41, doi: 10.1016/j.actaastro.2012.01.004.
[8] J. A. Atchison, M. A. Peck, A passive, sun-pointing, millimeter-scale solar sail, Acta Astronautica 67 (1-2) (2010) 108–121, doi: 10.1016/j.actaastro.2009.12.008.
[9] C. R. McInnes, Solar Sailing: Technology, Dynamics and Mission Applications, Springer-Praxis Series in Space Science and Technology, Springer-Verlag, Berlin, 1999, pp. 13–14, 46–54.
[10] C. Lücking, C. Colombo, C. R. McInnes, Electrochromic orbit control for smart-dust devices, Journal of Guidance, Control, and Dynamics 35 (5) (2012) 1548–1558, doi: 10.2514/1.55488.
[11] C. M. Lücking, C. Colombo, C. R. McInnes, Orbit control of high area-to-mass ratio spacecraft using electrochromic coating, in: 61st International Astronautical Congress, 2010, also paper IAC-10-C1.2.7.
[12] C. Colombo, C. Lücking, C. R. McInnes, Orbit evolution, maintenance and disposal of spacechip swarms through electrochromic control, Acta Astronautica 82 (1) (2013) 25–37, doi: 10.1016/j.actaastro.2012.05.035.
[13] G. Vulpetti, C. Circi, T. Pino, Coronal mass ejection early-warning mission by solar-photon sailcraft, Acta Astronautica 140 (2017) 113–125, doi: 10.1016/j.actaastro.2017.07.042.
[14] C. Colombo, C. R. McInnes, Orbital dynamics of "Smart-Dust" devices with solar radiation pressure and drag, Journal of Guidance, Control, and Dynamics 34 (6) (2011) 1613–1631, doi: 10.2514/1.52140.
[15] G. Mengali, A. A. Quarta, Heliocentric trajectory analysis of sun-pointing smart dust with electrochromic control, Advances in Space Research 57 (4) (2016) 991–1001, doi: 10.1016/j.asr.2015.12.017.
[16] G. Mengali, A. A. Quarta, E. Denti, Relative motion of sun-pointing smart dust in circular heliocentric orbits, Journal of Guidance, Control, and Dynamics (in press) doi: 10.2514/1.G003088.
[17] H. D. Curtis, Orbital Mechanics for Engineering Students, 3rd Edition, Elsevier Aerospace Engineering, Butterworth-Heinemann, 2014, Ch. 6, pp. 312–317, ISBN: 978-0-08-097747-8.
[18] J. L. Wright, Space Sailing, Gordon and Breach Science Publisher, Berlin, 1992, pp. 223–226.
[19] B. Dachwald, G. Mengali, A. A. Quarta, M. Macdonald, Parametric model and optimal control of solar sails with optical degradation, Journal of Guidance, Control, and Dynamics 29 (5) (2006) 1170–1178, doi: 10.2514/1.20313.
[20] B. Dachwald, M. Macdonald, C. R. McInnes, G. Mengali, A. A. Quarta, Impact of optical degradation on solar sail mission performance, Journal of Spacecraft and Rockets 44 (4) (2007) 740–749, doi: 10.2514/1.21432.
[21] G. Mengali, A. A. Quarta, C. Circi, B. Dachwald, Refined solar sail force model with mission application, Journal of Guidance, Control, and Dynamics 30 (2) (2007) 512–520, doi: 10.2514/1.24779.
[22] C. R. McInnes, Azimuthal repositioning of payloads in heliocentric orbit using solar sails, Journal of Guidance, Control, and Dynamics 26 (4) (2003) 662–664, doi: 10.2514/2.5098.
[23] G. Mengali, A. A. Quarta, In-orbit repositioning of multiple solar sail spacecraft, Aerospace Science and Technology 12 (7) (2008) 506–514, doi: 10.1016/j.ast.2007.12.003.
[24] A. E. Bryson, Y. C. Ho, Applied Optimal Control, Hemisphere Publishing Corporation, New York, NY, 1975, Ch. 2, pp. 71–89, ISBN: 0-891-16228-3.
[25] R. F. Stengel, Optimal Control and Estimation, Dover Publications, inc., 1994, pp. 222–254.
[26] G. Mengali, A. A. Quarta, Optimal three-dimensional interplanetary rendezvous using nonideal solar sail, Journal of Guidance, Control, and Dynamics 28 (1) (2005) 173–177, doi: 10.2514/1.8325.